Modelling of an industrial autothermal nylon-6 flow reactor

G. M. Ramesh and Santosh K. Gupta*
Department of Chemical Engineering, Indian Institute of Technology, Kanpur 208016, India
(Received 5 February 1992; revised 8 June 1992)

Mass- and energy-balance equations that describe the hydrolytic polymerization of nylon-6 in an autothermal industrial reactor are written. These account for both axial and radial variations of the temperature, as well as of the concentrations of the various molecular species. The set of coupled, non-linear partial differential equations are transformed into a set of ordinary differential equations (ODEs) using the finite-difference technique in the radial direction. The resulting stiff ODEs are then solved using Gear's algorithm. The method of successive substitutions is used to obtain convergence to the final results. Sharp radial gradients in temperature and average molecular weights are observed because of near-equilibrium conversions at the reactor walls and the low thermal conductivity of the reaction mass. It is demonstrated that these need to be accounted for in the proper design and analysis of reactors having this configuration. The effects of various operating conditions and parameters are studied. It is found that the hot-spot is parametrically sensitive to the feed-water concentration and to the presence of monofunctional acid in the feed. In addition, product having the same molecular weight can be obtained using two different feed-water concentrations. The results are found to be sensitive to the values of the heat transfer coefficients, and so good estimates of this parameter are required for simulation purposes.

(Keywords: polymerization; nylon; reaction engineering; modelling; autothermal reactor)

INTRODUCTION

The hydrolytic polymerization of ε-caprolactam is an important commercial process and has drawn the attention of many researchers. The work done has formed the subject of some recent reviews[1–4]. The mechanism and kinetics of polymerization are quite well established. In addition, several studies exist on the simulation of ideal reactors of various kinds. The emphasis these days appears to have shifted to the simulation and optimization of large-scale industrial reactors, several of which have been described by Sittig[5]. Computer simulations based on mathematical modelling of such polymerization reactors[6–8] or their combinations offer information that is of considerable importance for quality control and operational optimization of existing plants, as well as for the design of new plants.

This study is along this direction and models an existing industrial nylon-6 reactor in India. The reactor configuration is shown schematically in *Figure 1a*. The reactor is autothermal (i.e. the exothermic heat of reaction released is used to preheat the feed), and so is energy- and cost-efficient. However, this reactor is associated with the problem of parametric sensitivity (i.e. the maximum temperature or the 'hot-spot' temperature is sensitive to small changes in the values of some parameters, e.g. water concentration in the feed). This necessitates careful design as well as operation. This is why the development of a good model for this reactor is extremely important. The model presented in this paper explains the major trends of industrial reactor data.

A simple model was developed for this reactor in our earlier study[6], which showed that the hot-spot was extremely sensitive to the feed-water concentration under certain conditions. In addition, this study revealed that one could obtain products having identical molecular weights using two different values of the feed-water concentration. In one case, the temperature maximum is large, while in the other the temperature does not shoot up as significantly. The actual performance of the industrial reactor did, indeed, show the *qualitative* trends predicted by our preliminary model. A need arose, therefore, to improve the model of this reactor and to incorporate radial variations of temperature. This effect is quite significant since the thermal conductivity of the reaction mass is low. Even though computationally more expensive, such an improved and detailed model has the advantage of reflecting the conditions in the reactor more accurately. Moreover, such a model could be used to obtain optimal conditions of operation and thus to explore possibilities of cost reduction. As an illustration, we could use Pontryagin's minimum principle to obtain optimal jacket-fluid temperature profiles that would maximize the monomer conversion while simultaneously producing polymer having the desired molecular weight.

FORMULATION

The geometrical model used in this study is shown in *Figure 1b*. The helical tube shown in *Figure 1a* is difficult to model, and so is replaced by an *equivalent* concentric, hollow cylindrical region corresponding to $R_1 \leqslant r \leqslant R_2$ and referred to as reactor 2. Feed consisting of

* To whom correspondence should be addressed

0032-3861/93/081716-13
© 1993 Butterworth-Heinemann Ltd.

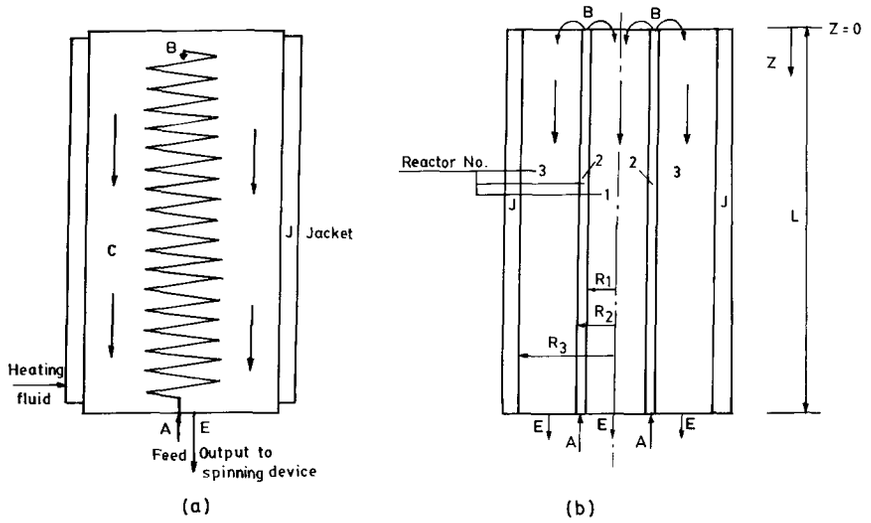

Figure 1 (a) Schematic representation of the industrial nylon-6 reactor simulated in this work and (b) the model used

ε-caprolactam (C_1), water (W) and, at times, monofunctional acetic acid (A_1) enters reactor 2 at the bottom (A in *Figure 1*) and flows straight up. The reactants are preheated to a temperature of 220–260°C as they flow upwards, and some amount of reaction also takes place. At the top (point B in *Figure 1*), the reaction mass flows out of the helical tube and flows down its outside. In our geometrical model (*Figure 1b*) of the actual reactor, the material flowing out of reactor 2 flows down in both reactors 1 and 3. Reactor 1 is cylindrical, while reactor 3 is a cylindrical annulus. The reaction mixture is assumed to get distributed in such a manner that the pressure drops along the length of these two reactors are equal. It is assumed that there is no exchange of mass between the three reactors except at point B. This is an approximation of the actual flow pattern, in which a small amount of transfer of material could occur between the inner and outer sides of the helical tube (i.e. between reactors 1 and 3) through the interstices in the coil. One could incorporate some lateral mixing mathematically to see its effect on the performance of the reactor, but this is not done since we expect this effect to be small.

As the reaction mass flows down in the tubular reactor 1, it exchanges heat with the material flowing countercurrently in the annular reactor 2. The reaction mass in the outer annular reactor 3 similarly exchanges heat with the material flowing upwards in reactor 2, as well as with the fluid in the jacket (J). The major part of the polymerization takes place in reactors 1 and 3, and the number-average chain length, μ_n, increases to the desired value by the time the reaction mass reaches the exit, E (at $Z = L$).

It is important to establish, at least approximately, the mathematical equivalence between the helical coil in the actual reactor and the concentric annular reactor 2 of its geometrical analogue shown in *Figure 1b*. In particular, the values of R_1 and R_2 need to be related to the coil dimensions of the physical reactor. The volume of reactor 2 ($= \pi(R_2^2 - R_1^2)L$) can be equated with the actual coil volume (the length, L, being the same for reactors 1 and 3 as well as for the actual reactor). Similarly, the surface area across which heat transfer takes place ($= 2\pi(R_2 + R_1)L$) in the model can be equated with the actual heat transfer area of the helical coil. These equations are sufficient to specify the two variables, R_1 and R_2. These two equations ensure that the surface-to-volume ratio of the geometrical model matches that of the physical reactor, and so the results predicted using the geometrical model will be meaningful. The axial velocity of the reaction mass in reactor 2 can be estimated using the feed flow rate ($\pi(R_2^2 - R_1^2)V_{2,f}$ = volumetric feed flow rate). This simultaneously ensures that the mean residence time of the reaction mixture in reactor 2 of the geometrical model matches that in the coil of the actual reactor. The heat transfer coefficients associated with the geometrical model must be taken to be those associated with the flow of the reaction mixture in the coil, to ensure validity of the results.

The kinetic scheme for the hydrolytic polymerization of ε-caprolactam to nylon-6 is presented in *Table 1*. This comprises the following three main reactions, ring opening, polycondensation and polyaddition, as well as the reactions with monofunctional acid molecules, A_n. The most important among the side reactions is the formation of cyclic oligomers since these adversely affect product properties. These reactions are included in *Table 1* as reactions 5 and 6. The reactions with higher cyclic oligomers are not incorporated in this scheme since the formation of cyclic dimer predominates and precise rate constants are not available yet for higher cyclic oligomers. The rate and equilibrium constants[2] are given in *Table 2*. *Table 3* gives the rate of formation, $\dot{\xi}_i$, of the various species and moments (ξ_i are defined in *Table 3*), while *Table 4* gives the net forward rate, $R_{r,i}$, associated with each of the six reactions in *Table 1*. These terms are used in the mass- and energy-balance equations for the reactor, given later. Closure equations commonly used to break the hierarchy of equations[3,9] are also listed in *Table 4*. All these equations are quite easily derived and are available in our earlier work[3,9,10].

The density ρ (and so the velocity), and the specific heat, C_p, of the reaction mixture vary with position because of changes in temperature and concentration. Correlations for these physical properties are given[11] in *Table 5*. The thermal conductivity of the reaction mass, k, is almost constant and its value is also included in

Table 1 Kinetic scheme for nylon-6 polymerization

1. Ring opening

$$C_1 + W \underset{k_1 = k_1/K_1}{\overset{k_1}{\rightleftharpoons}} S_1$$

2. Polycondensation

$$S_n + S_m \underset{k_2 = k_2/K_2}{\overset{k_2}{\rightleftharpoons}} S_{n+m} + W$$

3. Polyaddition

$$S_n + C_1 \underset{k_3 = k_3/K_3}{\overset{k_3}{\rightleftharpoons}} S_{n+1}$$

4. Reaction with monofunctional acid

$$S_n + A_m \underset{k_2}{\overset{k_2}{\rightleftharpoons}} A_{n+m} + W$$

5. Ring opening of cyclic dimer

$$C_2 + W \underset{k_4 = k_4/K_4}{\overset{k_4}{\rightleftharpoons}} S_2$$

6. Polyaddition of cyclic dimer

$$S_n + C_2 \underset{k_5 = k_5/K_5}{\overset{k_5}{\rightleftharpoons}} S_{n+2}$$

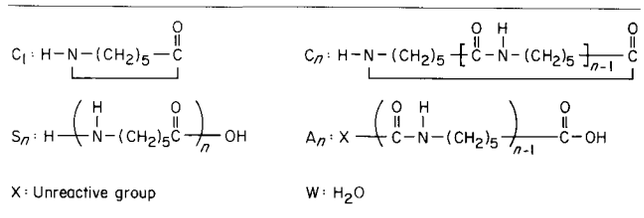

Table 5. The overall heat transfer coefficients, U, are assumed to be constant in this study and fall in the range typically encountered in nylon-6 reactors. Estimates of the heat transfer coefficient for a *different* reactor configuration[7,8] (an industrial semibatch reactor) indicate that its value drops by a factor of about 4–5 as the monomer conversion increases to near-equilibrium values. It was realized in our previous study[7,8] that existing correlations for the heat transfer coefficient are quite unreliable, and one needs to obtain its value either experimentally or by curve-fitting industrial reactor data. In view of this, we have assumed constant values for this parameter for the present reactor, and have generated results using different values to see if they are sensitive to this parameter.

Mass- and energy-balance equations for steady-state operation of the reactor, along with appropriate initial and boundary conditions, are given in *Tables 6–8*. Separate equations for reactors 1–3 have to be written. The equations for reactor 2 assume a plug-flow velocity profile and neglect radial temperature variations, this assumption being justified on the basis of the coil being thin. The equations for reactor 2 are, therefore, first-order ordinary differential equations (ODEs) and require one initial condition (feed condition) on each variable for integration. The concentrations and moments are, thus, functions of Z only.

The equations for reactor 1 given in *Table 6* are written assuming that the (laminar) velocity profile[12,13] is

Table 2 Rate and equilibrium constants

$$k_i = k_i^0 + k_i^c[\text{-COOH}] = A_i^0 \exp(-E_i^0/RT) + A_i^c \exp(-E_i^c/RT)[\text{-COOH}]$$

$$\equiv k_i^0 + k_i^c \sum_{n=1}^{\infty} ([S_n] + [A_n])$$

$$K_i = \exp(\Delta S_i/R - \Delta H_i/RT) \qquad i = 1, 2, \ldots, 5$$

i	A_i^0 (kg mol^{-1} h^{-1})	E_i^0 (J mol^{-1})	A_i^c (kg^2 mol^{-2} h^{-1})	E_i^c (J mol^{-1})	ΔH_i (J mol^{-1})	ΔS_i (J mol^{-1} K^{-1})
1	5.9874×10^5	8.3170×10^4	4.3075×10^7	7.8864×10^4	8.0249×10^3	-3.2989×10^1
2	1.8942×10^{10}	9.7365×10^4	1.2114×10^{10}	8.6483×10^4	-2.4877×10^4	3.9846
3	2.8558×10^9	9.5583×10^4	1.6377×10^{10}	8.4127×10^4	-1.6919×10^4	-2.906×10^1
4	8.5778×10^{11}	1.7573×10^5	2.3307×10^{12}	1.5648×10^5	-4.0166×10^4	-6.0751×10^1
5	2.5701×10^8	8.9119×10^4	3.0110×10^9	8.5353×10^4	-1.3259×10^4	2.4378

Table 3 Equations for the rate of formation of various species and moments

$$[\dot{C}_1] = -k_1[C_1][W] + k_1'[S_1] - k_3[C_1]\mu_0 + k_3'(\mu_0 - [S_1])$$

$$[\dot{S}_1] = k_1[C_1][W] - k_1'[S_1] - 2k_2[S_1]\mu_0 + 2k_2'[W](\mu_0 - [S_1]) - k_3[S_1][C_1] + k_3'[S_2] - k_2\mu_0'[S_1] + k_2'[W](\mu_0' - [A_1]) - k_5[S_1][C_2] + k_5'[S_3]$$

$$[\dot{C}_2] = -k_4[C_2][W] + k_4'[S_2] - k_5[C_2]\mu_0 + k_5'(\mu_0 - [S_1] - [S_2])$$

$$[\dot{W}] = -k_1[C_1][W] + k_1'[S_1] + k_2\mu_0^2 - k_2'[W](\mu_1 - \mu_0) + k_2\mu_0\mu_0' - k_2'[W](\mu_1' - \mu_0') - k_4[C_2][W] + k_4'[S_2]$$

$$[\dot{A}_1] = -k_2[A_1]\mu_0 + k_2'[W](\mu_0' - [A_1])$$

$$\dot{\mu}_0 = k_1[C_1][W] - k_1'[S_1] - k_2\mu_0^2 + k_2'[W](\mu_1 - \mu_0) - k_2\mu_0\mu_0' + k_2'[W](\mu_1' - \mu_0') + k_4[W][C_2] - k_4'[S_2]$$

$$\dot{\mu}_1 = k_1[C_1][W] - k_1'[S_1] + k_3[C_1]\mu_0 - k_3'(\mu_0 - [S_1]) - k_2\mu_0'\mu_1 - k_2'[W](\mu_1' - \mu_2')/2 + 2k_5[C_2]\mu_0 - 2k_5'(\mu_0 - [S_1] - [S_2]) + 2k_4[W][C_2] - 2k_4'[S_2]$$

$$\dot{\mu}_1' = k_2\mu_1\mu_0' - k_2'[W](\mu_2' - \mu_1')/2$$

$$\dot{\mu}_2 = k_1[C_1][W] - k_1'[S_1] + 2k_2\mu_1^2 + k_2'[W](\mu_1 - \mu_3)/3 + k_3[C_1](\mu_0 + 2\mu_1) + k_3'(\mu_0 - 2\mu_1 + [S_1]) - k_2\mu_2\mu_0' + k_2'[W](2\mu_3' - 3\mu_2' + \mu_1')/6 + 4k_5[C_2](\mu_1 + \mu_0) + 4k_5'(\mu_0 - \mu_1 + [S_2]) + 4k_4[W][C_2] - 4k_4'[S_2]$$

$$\dot{\mu}_2' = k_2(2\mu_1\mu_1' + \mu_2\mu_0') - k_2'[W](4\mu_3' - 3\mu_2' - \mu_1')/6$$

$$\dot{\mu}_0' = 0 \quad \text{or} \quad \mu_0' = \text{constant (= inlet value of } [A_1])$$

$$\xi \equiv [[C_1], [S_1], [C_2], [W], [A_1], \mu_0, \mu_1, \mu_1', \mu_2, \mu_2']$$

unidirectional (i.e. no mixing in radial direction), and that heat transfer occurs primarily by conduction in the radial direction and by convection (flow) in the Z direction. These equations are similar to those written earlier[10] for a tubular reactor. In writing these equations, the radial diffusion of all the components has been neglected. While the diffusion of heavy polymer molecules may indeed be negligible, it is possible that the diffusion of lower-molecular-weight components, particularly monomer and water, may not be so. Models paralleling those of Hamer and Ray[14] could be adapted to account for this effect. In this study, the diffusion of all components is neglected, since the radial diffusion is expected to be a second-order effect. A radial temperature gradient will be established in the reactor at any cross-section along the length because of the presence of a velocity profile as well as due to heat exchange with reactor 2 and the jacket. As a consequence, the concentrations of all the species and the moments will have radial as well as axial dependence. To obtain the concentration and temperature profiles the set of partial differential equations (PDEs) need to be solved. This is done using the finite-difference technique[15] in the radial direction, with the resultant ODEs being solved using Gear's technique[15]. The initial conditions (at $Z = 0$) are based on continuity of material flowing out of reactor 2. The boundary conditions in the radial direction are obtained by assuming a symmetric temperature profile at the centre-line of reactor 1 and the continuity of heat flux at the interface (wall) of reactors 1 and 2. The indeterminate form of the equations obtained at the centre-line on application of the finite-difference technique is solved by using L'Hospital's rule, as discussed earlier[10].

Table 8 shows the mass- and heat-balance equations for reactor 3. The velocity profile in this reactor at $Z = 0$ is that corresponding to laminar flow in an annulus (the

Table 4 Rates of reaction and closure conditions

Rates of reactions

$$R_{r,1} = k_1[C_1][W] - k_1'[S_1]$$
$$R_{r,2} = k_2\mu_0^2 - k_2'[W](\mu_1 - \mu_0)$$
$$R_{r,3} = k_3[C_1]\mu_0 - k_3'(\mu_0 - [S_1])$$
$$R_{r,4} = k_2\mu_0\mu_0' - k_2'[W](\mu_1' - \mu_0')$$
$$R_{r,5} = k_4[C_2][W] - k_4'[S_2]$$
$$R_{r,6} = k_5[C_2]\mu_0 - k_5'(\mu_0 - [S_1] - [S_2])$$

Closure conditions

$$[S_1] = [S_2] = [S_3]$$
$$\mu_3 = \frac{\mu_2(2\mu_2\mu_0 - \mu_1^2)}{\mu_1\mu_0}$$
$$\mu_3' = \frac{\mu_2'[2\mu_2'\mu_0' - (\mu_1')^2]}{\mu_1'\mu_0'}$$

Table 6 Mass- and energy-balance equations for reactor 1

$$\frac{\partial}{\partial Z}(\rho V_1) = 0$$
$$\frac{\partial}{\partial Z}(\rho V_1 \xi_{i,1}) = \rho\dot{\xi}_{i,1} \qquad i = 1, \ldots, 10$$
$$\frac{\partial}{\partial Z}(\rho C_p V_1 T_1) = \left(\frac{1}{r}\right)\frac{\partial}{\partial r}\left(rk\frac{\partial T_1}{\partial r}\right) + \rho\sum_{i=1}^{6}(-\Delta H_{r,i})R_{r,i}$$

Initial and boundary conditions

(i) $Z = 0,\ 0 \leqslant r \leqslant R_1$

$$T_1 = T_2$$
$$\xi_{i,1} = \xi_{i,2}$$
$$f = \frac{R_1^4}{R_3^2(R_3^2 - R_2^2)\left(\dfrac{1-(R_2/R_3)^4}{1-(R_2/R_3)^2} - \dfrac{1-(R_2/R_3)^2}{\ln(R_3/R_2)}\right)}$$
$$\bar{V}_1 = V_2\left(\frac{R_2^2 - R_1^2}{R_1^2}\right)\frac{f}{1+f}$$
$$V_1 = 2\bar{V}_1[1 - (r/R_1)^2]$$

(ii) $r = 0$

$$\partial T_1/\partial r = 0$$

(iii) $r = R_1$

$$-k\,\partial T_1/\partial r = U_1(T_1 - T_2)$$

$V_1 \to V_1(r, Z)$ $\quad \xi_{i,1} \to \xi_{i,1}(r, Z)$

$T_1 \to T_1(r, Z)$ $\quad \rho \to \rho(r, Z)$

$T_2 \to T_2(Z)$ $\quad C_p \to C_p(r, Z)$

Table 7 Mass- and energy-balance equations for reactor 2

$$-\frac{d}{dZ}(\rho V_2) = 0$$
$$-\frac{d}{dZ}(\rho V_2 \xi_{i,2}) = \rho\dot{\xi}_{i,2} \qquad i = 1, 2, \ldots, 10$$
$$\frac{d}{dZ}(\rho C_p V_2 T_2) = 2\pi R_1 U_1[T_2 - T_1(R_1, Z)]/[\pi(R_2^2 - R_1^2)] + 2\pi R_2 U_2[T_2 - T_3(R_2, Z)]/[\pi(R_2^2 - R_1^2)] - \rho\sum_{i=1}^{6}(\Delta H_{r,i})R_{r,i}$$

Initial conditions

(i) $Z = L$

$$\xi_{i,2} = \xi_{i,f}$$
$$T_2 = T_f$$
$$V_2 = V_{2,f}$$

$V_2 \to V_2(Z)$ $\quad \xi_{i,2} \to \xi_{i,2}(Z)$

$T_1 \to T_1(r, Z)$ $\quad \rho \to \rho(Z)$

$T_2 \to T_2(Z)$ $\quad C_p \to C_p(Z)$

$T_3 \to T_3(r, Z)$

Table 5 Thermophysical properties[11]

$$\rho = \frac{1000}{1.0065 + 0.0123[C_1] + (T - 495)(0.000\,35 + 0.000\,07[C_1])} \qquad (\text{kg m}^{-3})$$
$$C_p = 4.816\{0.6593[C_1]/[C_1]_f + (1.0 - [C_1]/[C_1]_f)(0.4861 + 0.000\,337T)\} \qquad (\text{kJ kg}^{-1}\,\text{K}^{-1})$$
$$k = 0.281 \qquad (\text{W m}^{-1}\,\text{K}^{-1})$$

Table 8 Mass- and energy-balance equations for reactor 3

$$\frac{\partial}{\partial Z}(\rho V_3) = 0$$

$$\frac{\partial}{\partial Z}(\rho V_3 \xi_{i,3}) = \rho \dot{\xi}_{i,3} \qquad i = 1, 2, \ldots, 10$$

$$\frac{\partial}{\partial Z}(\rho C_p V_3 T_3) = \left(\frac{1}{r}\right)\frac{\partial}{\partial r}\left(rk\frac{\partial T_3}{\partial r}\right) + \rho \sum_{i=1}^{6} (-\Delta H_{r,i}) R_{r,i}$$

Initial and boundary conditions

(i) $Z = 0$, $R_2 \leqslant r \leqslant R_3$

$$T_3 = T_2$$

$$\xi_{i,3} = \xi_{i,2}$$

$$\bar{V}_3 = V_2\left(\frac{R_2^2 - R_1^2}{R_3^2 - R_2^2}\right)\frac{1}{1+f} \qquad (f \text{ from } \textit{Table 6})$$

$$\frac{V_3}{\bar{V}_3} = 2\frac{\left[1 - \left(\frac{r}{R_3}\right)^2 + \frac{1-(R_2/R_3)^2}{\ln(R_3/R_2)}\ln(r/R_3)\right]}{\left(\frac{1-(R_2/R_3)^4}{1-(R_2/R_3)^2} - \frac{1-(R_2/R_3)^2}{\ln(R_3/R_2)}\right)}$$

(ii) $r = R_2$

$$-k\,\partial T/\partial r = U_2[T_2 - T_3(R_2, Z)]$$

(iii) $r = R_3$

$$-k\,\partial T/\partial r = U_j[T_3(R_3, Z) - T_j]$$

$V_3 \rightarrow V_3(r, Z)$ $\quad \xi_{i,3} \rightarrow \xi_{i,3}(r, Z)$

$T_2 \rightarrow T_2(Z)$ $\quad \rho \rightarrow \rho(r, Z)$

$T_3 \rightarrow T_3(r, Z)$ $\quad C_p \rightarrow C_p(r, Z)$

equation for an incompressible fluid at the temperature at $Z = 0$ is used for this purpose). At any other axial position, the velocity is assumed to be such that the mass flow rate at any r is the same as the value (at that r) at $Z = 0$. It is assumed that the liquid coming out of reactor 2 divides itself into reactors 1 and 3 such that the pressure drop in the two reactors is identical. Again it is assumed for this purpose that the fluid is at constant temperature, that at $Z = 0$ (i.e. density changes are neglected). A similar approach as that used in reactor 1 is used to solve the set of partial differential equations. The boundary conditions for heat balance in the radial direction are different from that of reactor 1. The boundary conditions in the radial direction are the continuity of heat flux at the wall between the jacket (J) and reactor 3, and at the wall between reactors 2 and 3.

In true laminar flow, the residence time at the wall is infinity. To avoid numerical problems, a small slip ($V_i/\bar{V} = 1 \times 10^{-4}$) was assumed at the walls, in both reactors 1 and 3. It has been found[10] that use of this approximation does not affect the results much. The inlet conditions at the points $Z = 0$, $r = R_1$, R_2 and R_3 for reactors 1 and 3 were also modified to decrease numerical stiffness. The equilibrium conversion values for the isothermal run at 250°C were fed in as values at these points. This approximation has also been justified in our earlier study[10].

The ODEs obtained for reactors 1 and 3, using the finite-difference technique, form a coupled set with the ODEs for reactor 2. The algorithm used for solving these involves a successive-substitutions procedure[15], as described below:

(1) Initial *wall* temperature profiles, $T_1(R_1, Z)$ and $T_3(R_2, Z)$, at different values of Z, $0 \leqslant Z \leqslant L$, are assumed (isothermal).

(2) The ODEs for reactor 2 are integrated from $Z = L$ to $Z = 0$ using a double-precision version of the NAG library subroutine D02EBF (for the solution of stiff ODEs using Gear's method). The assumed temperature profiles, $T_1(R_1, Z)$ and $T_3(R_2, Z)$, are used. Linear interpolation is used for these temperatures where required.

(3) Values of ξ_i, the various molecular species and moments (defined in *Table 3*), velocity and temperature are obtained at different values of r at $Z = 0$, using the continuity equations given in *Tables 6* to *8*.

(4) The ODEs for reactors 1 and 3 are integrated from $Z = 0$ to $Z = L$ using the temperature profile in reactor 2 as computed in step (2). If the temperature, $T_2(Z)$, is required at a value of Z other than at which it is stored, it is obtained by interpolating linearly between the stored values.

(5) The computed temperatures, $T_1(R_1, Z)$ and $T_3(R_2, Z)$, are compared against the assumed values. If these agree within a tolerance, ERR TEMP, at all points, no further computations are required. If not, these computed values, $T_1(R_1, Z)$ and $T_3(R_2, Z)$, are used as the new assumed values (successive-substitutions method) in step (1) and the procedure is repeated till convergence. Mean or radially averaged values of various concentrations, moments and temperatures are obtained using the equations given in *Table 9* (these would be values obtained if the material from various radial locations were allowed to flow into a cup and mixed instantaneously; hence they are often referred to as 'cup-mixing' values).

RESULTS AND DISCUSSION

A general computer program was utilized to solve the set of equations described above. The assumed wall temperature profiles, $T_1(R_1, Z)$ and $T_3(R_2, Z)$, were taken to be isothermal at 523 K. Storage at every 1 m location was tried. A typical run using the reference values of the parameters as given in *Table 10* took 140 s CPU time on a supermini HP 9000/850S system. It is interesting to note that the successive-substitutions algorithm (Picard iteration on $T_1(R_1, Z)$ and $T_3(R_2, Z)$) proposed earlier did indeed converge, and so there was no necessity to use the Newton–Raphson technique,

Table 9 Mixture properties

$$\bar{\xi}_i(Z) = \frac{\int_0^{R_1} \rho V_1 r \xi_{i,1}\,dr + \int_{R_2}^{R_3} \rho V_3 r \xi_{i,3}\,dr}{\int_0^{R_1} \rho V_1 r\,dr + \int_{R_2}^{R_3} \rho V_3 r\,dr} \qquad i = 1, 2, \ldots, 10$$

$$\bar{T}(Z) = \frac{\int_0^{R_1} \rho V_1 r C_p T_1\,dr + \int_{R_2}^{R_3} \rho V_3 r C_p T_3\,dr}{\int_0^{R_1} \rho V_1 r C_p\,dr + \int_{R_2}^{R_3} \rho V_3 r C_p\,dr}$$

$$\bar{\mu}_n(Z) = \frac{\bar{\mu}_1(Z) + \bar{\mu}_1'(Z)}{\bar{\mu}_0(Z) + \bar{\mu}_0'(Z)}$$

$$\bar{\mu}_w(Z) = \frac{\bar{\mu}_2(Z) + \bar{\mu}_2'(Z)}{\bar{\mu}_1(Z) + \bar{\mu}_1'(Z)}$$

$$\bar{Q}(Z) = \frac{\bar{\mu}_w(Z)}{\bar{\mu}_n(Z)}$$

which usually has faster and better convergence characteristics, but requires derivatives.

The computer program developed was first checked against some results from our earlier studies. Results were generated for the plug-flow reactor 2 alone, ensuring that the temperature of the reaction mass all through was constant (i.e. the energy-balance equation was used with heat generation term taken as zero and $T_1(R_1, Z)$ and $T_3(R_2, Z)$ equal to the value of T_2 at the feed point). The results obtained were found to match those of Ray and Gupta[16] at different temperatures ranging from 230 to 270°C. This confirmed the correctness of the rate equations used in the program, as well as the logic used. Results were also generated for the plug-flow reactor 2 alone, assuming adiabatic operation ($U_1 = U_2 = 0$). These were found to match the results of Gupta and Tjahjadi[6] and Pal and Gupta[10] for similar conditions. The equations for the tubular reactor 1 were checked by simulating this reactor alone, assuming $T_2(Z)$ to be at a uniform value. Our results were found to be in agreement with those from our earlier study[10] under laminar-flow conditions.

With these tests completed, results were generated for the autothermal reactor for the *reference* conditions given in *Table 10*. These represent conditions for a relatively low-capacity industrial reactor operating in India, with a production capacity of about 15 tons per day. Three *computational* parameters were used in generating the results: the tolerance, TOL, specified for the Gear code D02EBF; the number, NG, of finite-difference grid points used in reactors 1 and 3 (the same number was used for both); and the maximum error, ERR TEMP, permitted at any Z in the values of the wall temperatures, $T_1(R_1, Z)$ and $T_3(R_2, Z)$ (this is the tolerance used to test convergence in the successive-substitutions algorithm). These computational parameters were varied around the reference values, and the results are shown in *Table 11*. The maximum local temperature in reactors 1 and 3, and the values of μ_n and monomer conversion, x, at the locations of these maxima in temperature, are found to be relatively unaffected by changes in the values of the computational parameters. *Table 11* also shows how the maximum (radially averaged) mean temperature in reactors 1 and 3 and the corresponding μ_n and monomer conversion are also unaffected by changes in these parameters. The choice of the computational parameters used for generating the reference results is thus justified.

Figures 2–6 show the axial variations of the (radially) averaged values of temperature, $\bar{T}$, monomer conversion, $\bar{x}$, number-average chain length, $\overline{\mu_n}$, polydispersity index, $\bar{Q}$, and cyclic dimer concentration, $\overline{[C_2]}$, in the autothermal reactor operating under the reference conditions given in *Table 10*. The cup-mixing values for reactors 1 and 3 together have been shown in these figures. Results are *qualitatively* similar to those obtained using our previous model[6] in which radial gradients were not accounted for (results for $\bar{Q}$ were not generated earlier, and are new). It may be mentioned that the reference values used in our earlier work were chosen so as to illustrate how, under certain conditions, this reactor could show parametrically sensitive behaviour (a pathological condition—which should really be avoided in a well designed system). The values selected in this work are more representative of the reactor under actual (and better) operation. It is observed from *Figure 2* that the temperature of the reaction mass increases by about 11°C as it flows up the coil (reactor 2). This is not, however, accompanied by much reaction (see *Figure 3*), and the values of $\bar{x}$ and $\overline{\mu_n}$ at the top ($Z = 0$) of the

Table 10 Reference values of the parameters and operating conditions

$[C_1]_f$	8.8 mol kg^{-1}
$[W]_f$	0.15 mol kg^{-1}
$[A_1]_f$	0.0 mol kg^{-1}
$[C_2]_f$	0 mol kg^{-1}
$[S_1]_f = \mu_{0,f} = \mu'_{0,f} = \mu_{1,f} = \mu'_{1,f}$ $= \mu_{2,f} = \mu'_{2,f} = 0.0$ mol kg^{-1}	
$V_{2,f}$	12.0 m h^{-1}
T_f	488.0 K
L	20.0 m
R_1	0.175 m
R_2	0.20 m
R_3	0.40 m
T_j	530 K
U_1	5.81 W m^{-2} K^{-1}
U_2	5.81 W m^{-2} K^{-1}
U_j	23.23 W m^{-2} K^{-1}
Number, NG, of grid points in each of reactors 1 and 3	11
Tolerance, TOL (for integration in D02EBF)	10^{-4}
Slip at the walls as fraction of mean velocity	1×10^{-4}
Convergence parameter for temperature, ERR TEMP	0.25 K
Initial (trial) values of $T_1(R_1, Z)$ and $T_3(R_2, Z)$	523 K

Table 11 Results for different computational parameters

No.	TOL	NG	ERR TEMP (°C)	N_r[a]	T_{max} (°C)	μ_n at T_{max}	x (%) at T_{max}	$\bar{T}_{max}$ (°C)	μ_n at $\bar{T}_{max}$	$\bar{x}$ (%) at $\bar{T}_{max}$
1 (ref.)	10^{-4}	11	0.25	1	268.2239	105.1764	60.5477	263.4192	155.6100	81.5647
				3	274.5345	149.1140	78.4206			
2	10^{-4}	9	0.25	1	267.2964	102.1995	59.0598	263.2900	155.1290	81.2993
				3	274.4478	148.6015	80.0741			
3	10^{-4}	13	0.25	1	268.7029	108.7841	61.3407	263.4852	155.8676	81.7028
				3	274.5768	150.1298	80.7530			
4	10^{-3}	11	0.25	1	268.2116	105.1672	60.5457	263.4147	155.6079	81.5635
				3	274.5316	149.6164	80.5242			
5	10^{-4}	11	0.35	1	268.7284	107.0558	61.4702	263.533	155.9703	81.7557
				3	274.6464	150.1825	80.7882			
6	10^{-4}	11	0.15	1	267.9119	104.0719	59.9990	263.3469	155.3997	81.4510
				3	274.4620	149.2730	80.3642			

[a]Reactor number

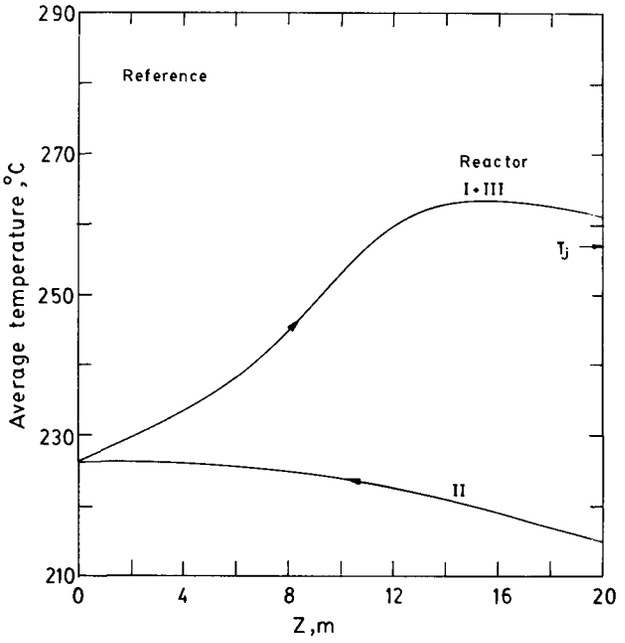

Figure 2 Variation of mean temperature of the reaction mass with axial position. Reference values of the parameters (*Table 10*) used

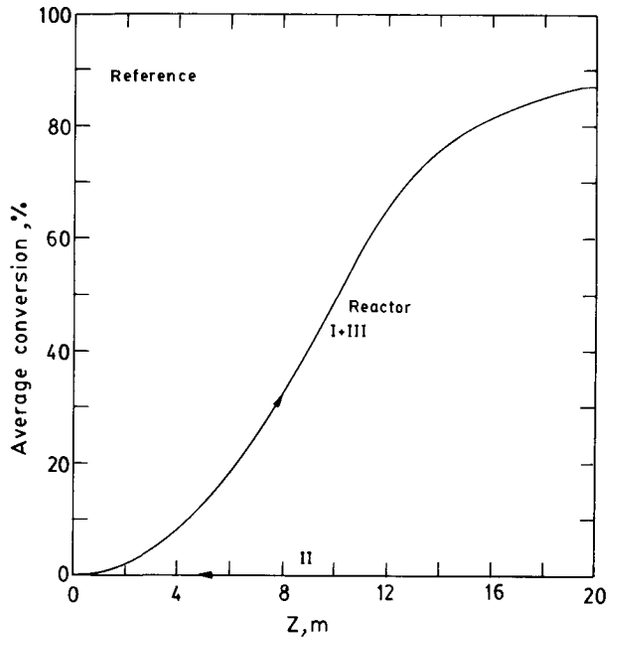

Figure 3 Axial variation of average monomer conversion (reference run)

autothermal reactor are quite low. This is because the velocities in reactor 2 are relatively large and the characteristic time-scales for chemical reaction are large as opposed to those for heat transfer. The mean temperature does rise by about 40°C as the reaction mass flows down on the outside of the coil, at much smaller velocities. A relatively flat maximum is observed in the mean temperature (*Figure 2*) somewhere before the exit. The values of $\bar{x}$ and $\overline{\mu_n}$ continue to increase even beyond this point as the reaction mass flows down further. The existence of a maximum in $\bar{T}$ is because of the fact that the jacket fluid is able to carry away the exothermic heat of reaction released beyond its locations sufficiently rapidly in reactor 3 since the reaction is not so fast beyond this point.

It is interesting to observe the relatively high values of $\bar{Q}$ (average polydispersity index) somewhere near the top of the reactor. Values of $\bar{Q}$ as high as about 4.2 are observed. This is because of a *mixing effect* associated with averaging of polymers having very different values of μ_n (see *Figure 7*). After some position the value of $\bar{Q}$ decreases to its expected value of about 2.0, as the range of values of μ_n in reactors 1 and 3 becomes smaller. *Figures 7–11* show the radial variation of the number-average chain length, temperature, monomer conversion, polydispersity index and cyclic dimer concentration. These results show significant radial variations, which were neglected in our earlier *lumped-parameter* model[6]. In fact, these radial variations are found to be quite large even at the exit, $Z = 20$ m.

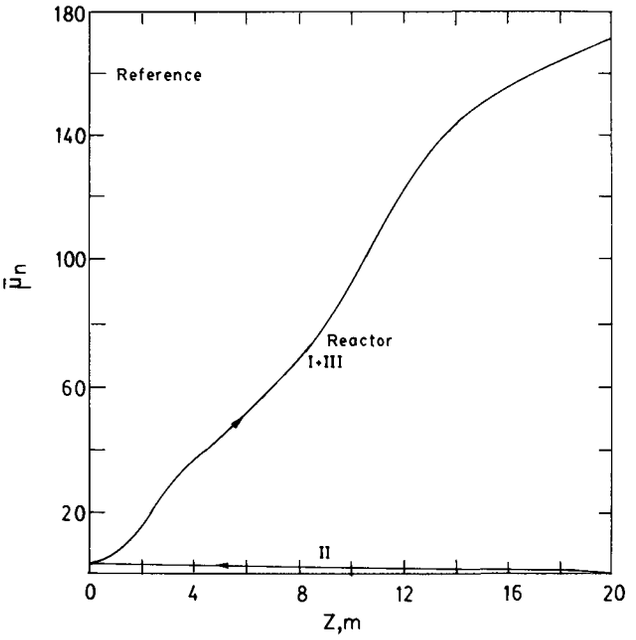

Figure 4 Axial variation of average values of μ_n (reference run)

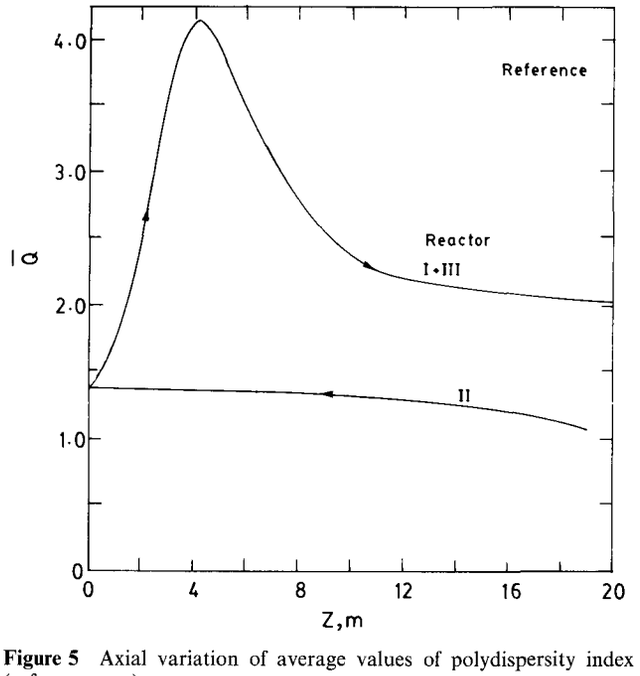

Figure 5 Axial variation of average values of polydispersity index (reference run)

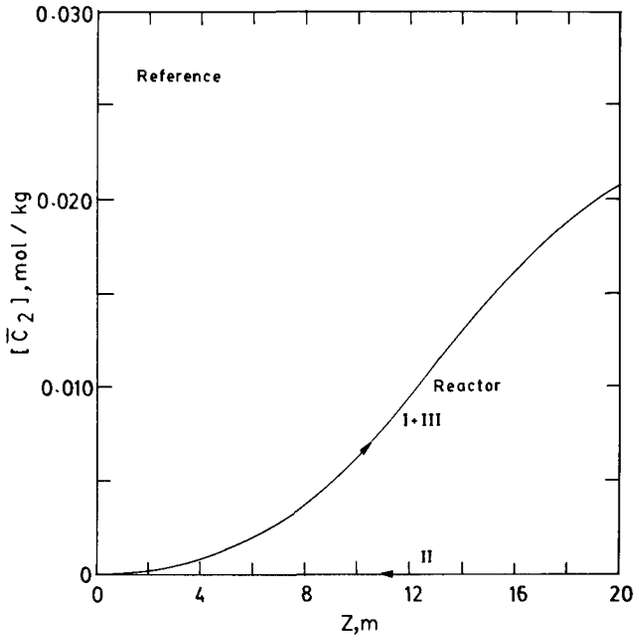

Figure 6 Axial variation of cyclic dimer concentration (reference run)

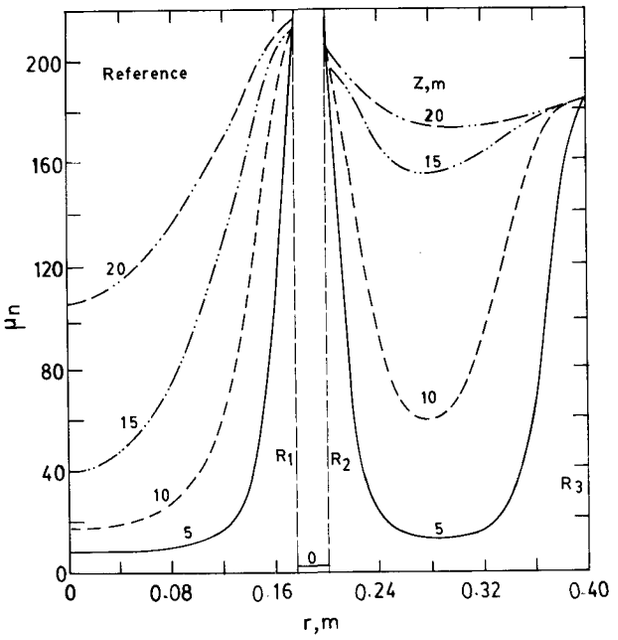

Figure 7 Radial variation of μ_n at five axial positions (reference run)

The radial variations have important ramifications in terms of product properties and reactor design. For the reference run, it is observed that the highest value, T_{max}, of the *local* temperature is about 10°C higher than the maximum value, $\bar{T}_{max}$, of the mean temperature. This difference could be unimportant for the reference run studied here (since T_{max} is only about 274°C). However, one could easily envisage operating conditions wherein $\bar{T}_{max}$ is below the upper limit (imposed by degradation reactions, etc.), while T_{max} is significantly above it. Our present model is, thus, observed to be superior to our earlier model[6] in that it can predict such possibilities.

The radial variations of the various quantities shown in *Figures 7–11* show trends that can be interpreted intuitively. Because of the laminar flow profile in reactor 1, the velocity near the centre is much higher than at the wall, and so the residence time of a fluid element near the wall ($r = R_1$) is higher (theoretically, infinite). Thus, one has near-equilibrium reaction conditions at the wall ($r = R_1$). *Figure 8* shows that a maximum is observed in the temperature slightly away from the wall at $Z = 5$ m. The higher temperature leads to thermal conduction inwards (as well as outwards) and, as Z increases, the temperature peak shifts inwards. The fluid elements at the wall in reactor 1 exchange heat with reactor 2, and since there is a decrease in the temperature in reactor 2 as one goes downwards, the *wall* temperature in reactor 1 falls along the length of the reactor. Similar temperature peaks are observed in reactor 3. However,

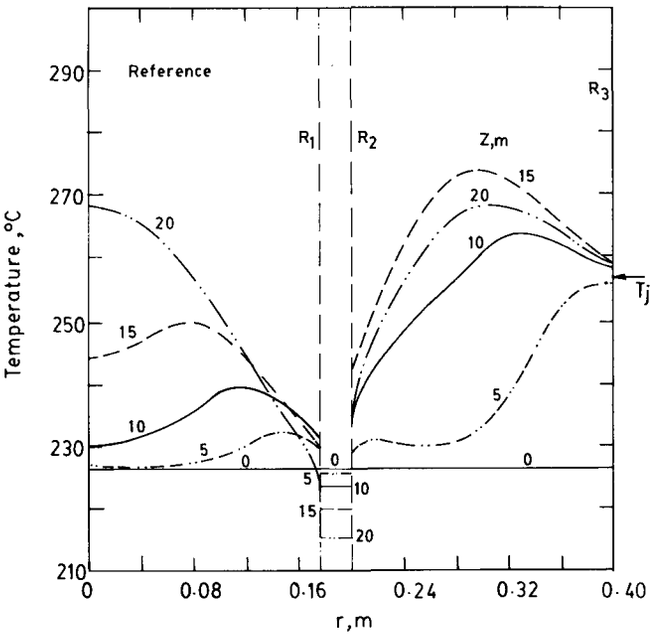

Figure 8 Radial variation of temperature at five axial positions (reference run)

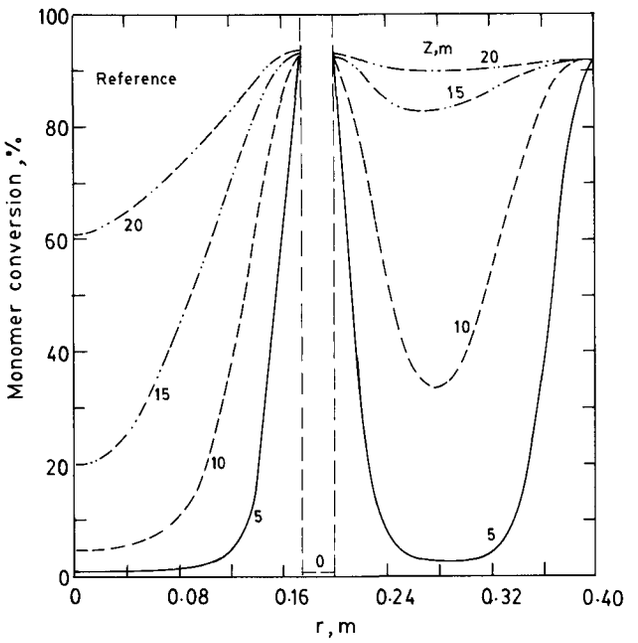

Figure 9 Radial variation of monomer conversion at five axial positions (reference run)

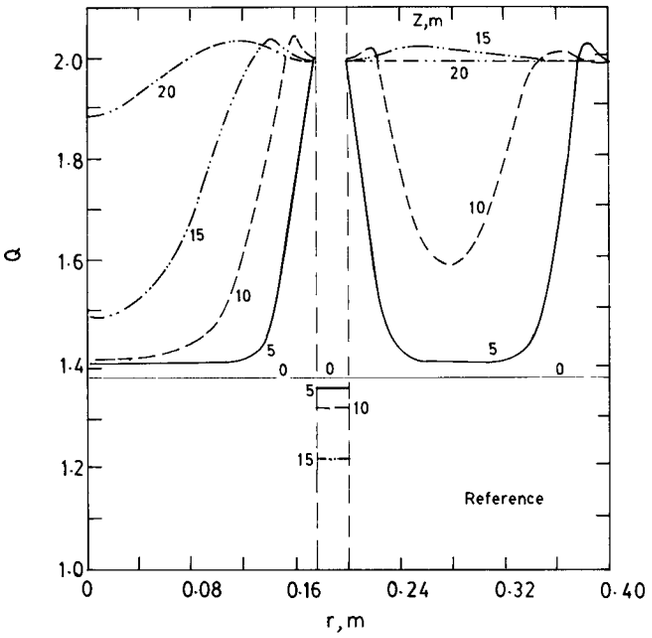

Figure 10 Radial variation of polydispersity index at five axial positions (reference run)

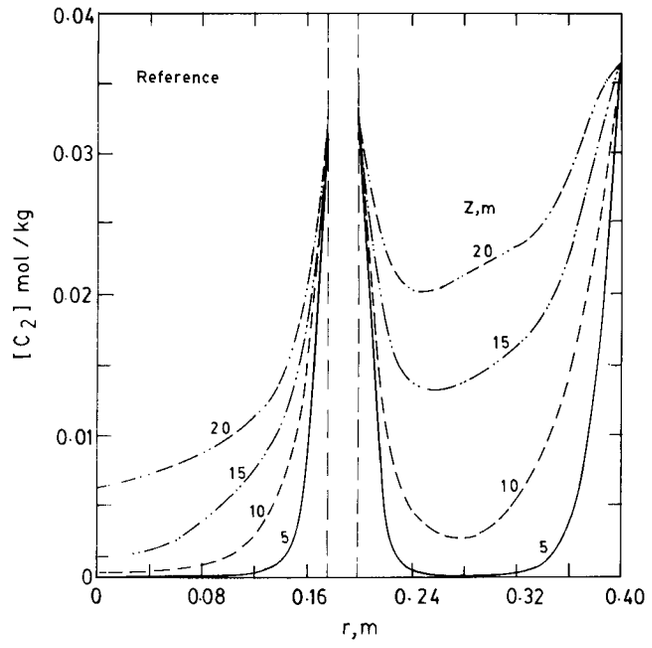

Figure 11 Radial variation of $[C_2]$ at five axial positions (reference run)

it is observed from *Figure 8* that, in this reactor, the temperatures are lower at $Z = 20$ m than at $Z = 15$ m. This is because not much reaction takes place in the zone $15\text{ m} \leqslant Z \leqslant 20\text{ m}$, as observed in *Figure 9*, and heat transfer predominates. It is interesting to observe that the maximum value of T_{max} (for $Z = 15$ m) is only about 10°C higher than the value of $\bar{T}_{max}$. This small difference is because, under the reference conditions used in this work, the reactor is not very parametrically sensitive. The minima in the values of μ_n in reactor 3 at any Z (see *Figure 7*) are because of the relatively higher velocities (and lower residence times) of fluid elements in these regions. These are also accompanied by minima in the monomer conversions, x, and in $[C_2]$ (see *Figures 9* and *11*). These minima become less accentuated as Z increases, the higher temperatures somewhat compensating for the lower residence times.

The various operating conditions and parameters were changed one at a time, keeping the others at their reference values, to find out which ones are most crucial in influencing reactor operation. Detailed (graphical) results are not being provided for reasons of brevity (but can be supplied on request). A summary of the results is given below:

(a) When the feed velocity, $V_{2,f}$, is decreased, the mean residence time increases, and $\bar{T}_{max}$ increases (by about 4°C for a change of $V_{2,f}$ from 12 to 11 m s^{-1}). The exit value of $\bar{T}$ and $\bar{Q}$ are not affected much, though $\overline{\mu_n}$ and $\overline{[C_2]}$ at the exit are found to increase.

(b) Decrease of the jacket temperature, T_j, from the reference value of 257°C to 247°C leads to a decrease in the values of $\bar{T}$ almost throughout the column (by about 5°C). This leads to a decrease in the values of $\overline{[C_2]}$, but values of $\overline{\mu_n}$, $\bar{x}$ and $\bar{Q}$ are not affected much. This suggests that one can obtain a better product (having lower undesirable cyclic dimer but the same $\overline{\mu_n}$) by lowering T_j, at least to some extent.

(c) In contrast to (b), reduction of the feed temperature, T_f, leads to a simultaneous lowering not only of $\bar{T}$, but also of $\bar{x}$, $\overline{\mu_n}$ and $\overline{[C_2]}$.

(d) Increase in the length, L, of the reactor from 20 m to 22 m leads to increases in $\bar{T}$ (as well as $\bar{T}_{max}$ by 3°C), $\bar{x}_{end}$ (from 88% to 90%), $\overline{\mu_{n,end}}$ (from 171 to 179) and $\overline{[C_2]}_{end}$.

(e) The effect of the feed-water concentration, $[W]_f$, is quite interesting. When $[W]_f$ is increased from 0.13 to 0.18 mol kg^{-1}, the final (at $Z = 20$ m) value of $\bar{T}$ is not affected much, though $\bar{T}_{max}$ increases monotonically (by about 7°C). The mean monomer conversion increases from about 81% at $[W]_f = 0.13$ mol kg^{-1} to about 90% at $[W]_f = 0.17$ mol kg^{-1}, and then remains almost unchanged with further increases in $[W]_f$. $\overline{[C_2]}_{end}$ is found to increase continuously with increasing $[W]_f$. A very interesting phenomenon is observed in the values of $\overline{\mu_n}$ of the product, as shown in *Figure 12*: $\overline{\mu_{n,end}}$ first increases as $[W]_f$ is increased from 0.13 to 0.14 mol kg^{-1}, and then decreases as $[W]_f$ is increased further. Thus, we can obtain the same molecular-weight product (say $\overline{\mu_{n,end}} = 169$) using two values of $[W]_f$, one associated with lower values of $\bar{T}_{max}$, $\bar{x}_{end}$ and $\overline{[C_2]}_{end}$, and the other with higher values of these quantities. This behaviour of the reactor enables an operator some kind of flexibility. The reason for this interesting behaviour is the interplay of kinetic and equilibrium effects. At low values of $[W]_f$, the sluggishness of the ring-opening reaction predominates, and increase of $[W]_f$ leads to an increase of polymerization, and to an associated increase in $\overline{\mu_{n,end}}$. After some value of $[W]_f$, equilibrium effects are dominant, and increasing $[W]_f$ leads to lower $\overline{\mu_n}$ products.

(f) It is extremely important to study the effect of the overall heat transfer coefficients, U_1, U_2 and U_j, on the polymerization, particularly since our earlier study on a semibatch industrial nylon-6 reactor[7,8] has established that estimates for these parameters are quite untrustworthy (indeed, in our simulation work on the semibatch reactor, we had curve-fitted the constant of proportionality in the relation between the Nusselt number and the Reynolds number, using actual data on the reactor). *Figure 13* shows the effect of U_1 ($= U_2$) on the $\bar{T}$ profiles.

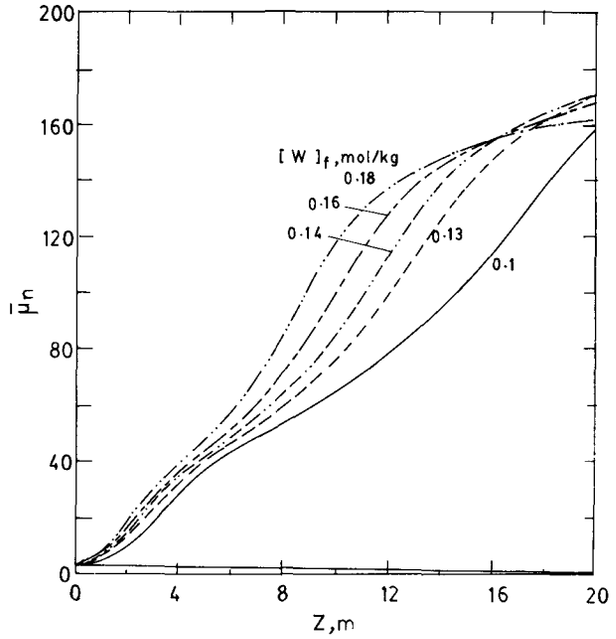

Figure 12 Variation of $\bar{\mu}_n$ with axial location as $[W]_f$ is changed. All other conditions are as given in *Table 10*

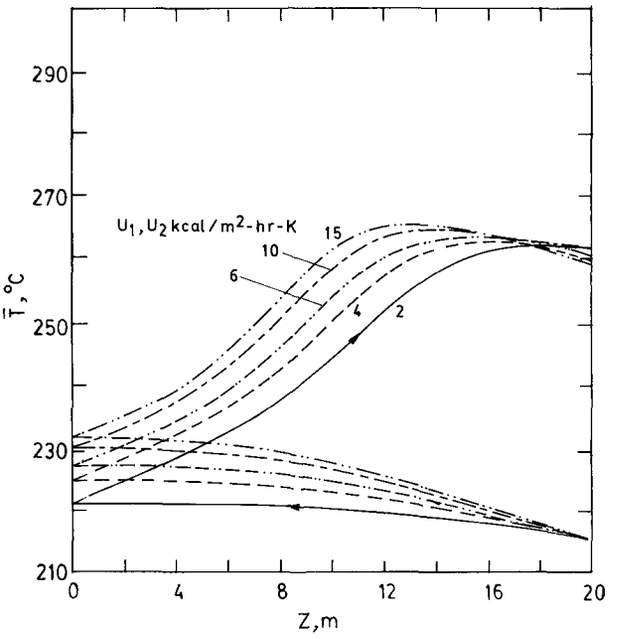

Figure 13 Effect of U_1 and U_2 ($U_1 = U_2$) on $\bar{T}$. All other conditions as in *Table 10*. Values of U_1 in W m^{-2} K^{-1} can be obtained by multiplying the given values by 1.162

It is found (not shown in figure) that the value of $\overline{\mu_{n,end}}$ varies from about 160 to 178 as U_1 increases from 2.32 to 17.43 W m^{-2} K^{-1}. The value of $\bar{x}_{end}$ also increases from about 83.5% to 89.5% in the same range of U_1. The importance of obtaining good estimates of U_1 and U_2 is, thus, again established. We expect that improvements will be achieved in modelling studies if we use the form of existing heat transfer correlations and use industrial reactor data to curve-fit 'constants' in them, as was done in our previous study[7,8]. Moreover, the lower viscosity of the reaction mass at low monomer conversions may lead to velocity profiles that are flatter than the parabolic forms assumed in this work, influencing, in turn, temperature and concentration profiles. It is believed, however, that these effects will cancel out at least partially. *Figure 13* suggests that larger initial values of U_1, followed by lower values near the end, would lead to almost the same final temperature. It is found that changing U_j from 11.62 to 34.863 W m^{-2} K^{-1} does not alter the results perceptibly.

Results were also generated with the feed incorporating 0.088 mol kg^{-1} of a monofunctional acid, A_1. The addition of A_1 speeds up the reaction, but at the cost of lower final values of $\overline{\mu_{n,end}}$, as shown in *Figures 14* and *15*. Higher initial rates also lead to higher temperatures, as shown in *Figure 16*, and one must be careful to ensure that local temperatures that are higher than $\bar{T}_{max}$ do not go too high to start degradation reactions. The hot-spot temperature and location are both found to be quite sensitive to the value of $[A_1]_f$.

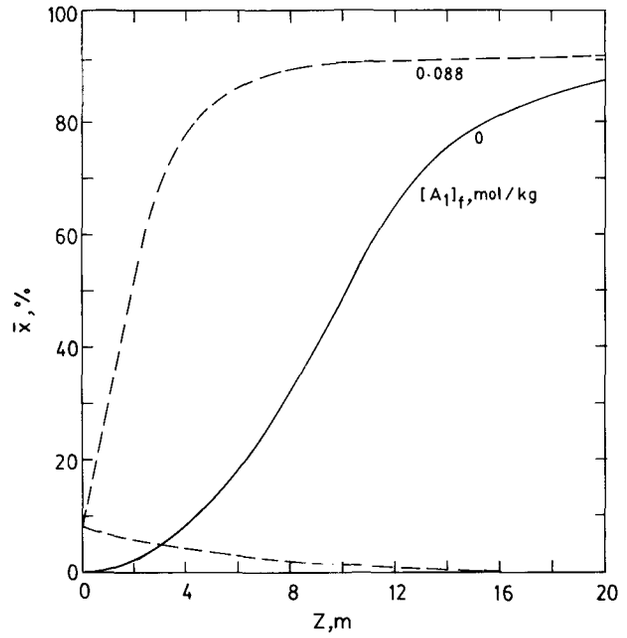

Figure 14 Effect of $[A_1]_f$ on the mean monomer conversion. All other parameters as in *Table 10*

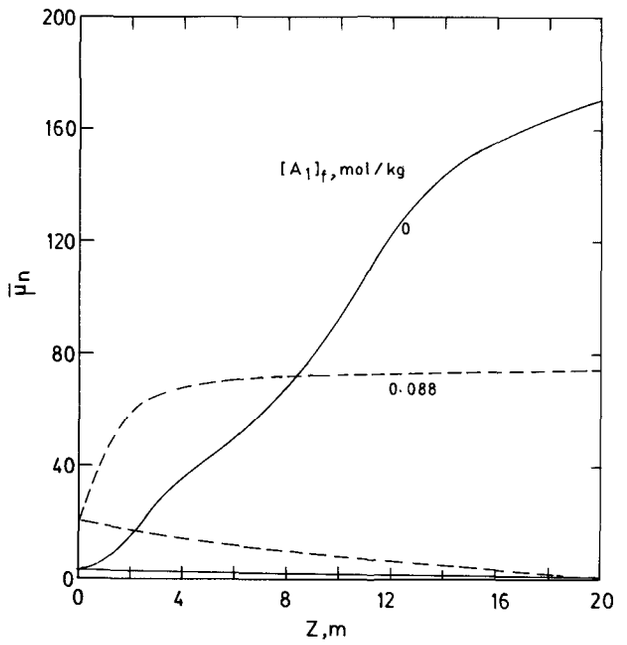

Figure 15 Effect of $[A_1]_f$ on $\bar{\mu}_n$. Other variables as in *Table 10*

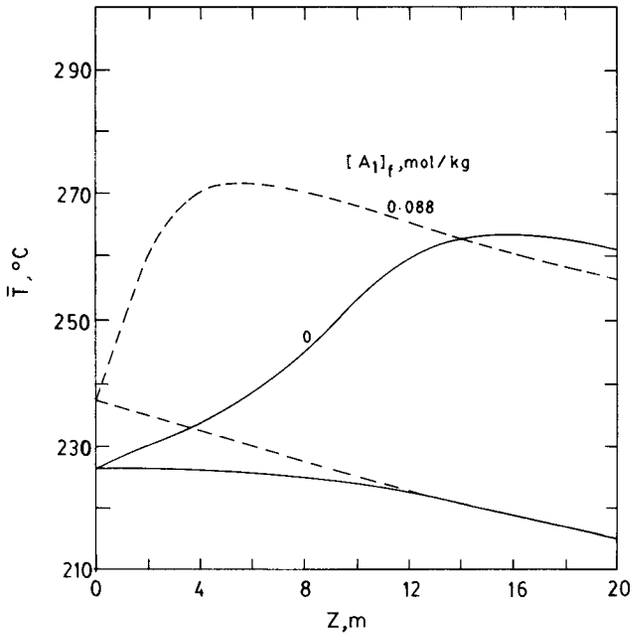

Figure 16 Effect of $[A_1]_f$ on $\bar{T}$. All other conditions as in *Table 10*

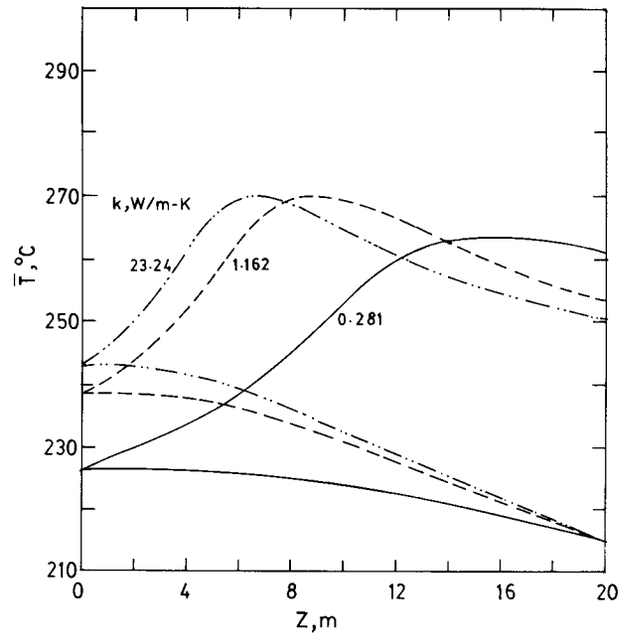

Figure 17 Effect of changing k on $\bar{T}$. As k goes to infinity, the model reduces to the earlier lumped model

Figure 17 shows how the $\bar{T}$ profile changes as the thermal conductivity, k, is increased from the actual values of 0.281 W m^{-1} K^{-1} to 23.24 W m^{-1} K^{-1}. As k is increased, the radial variations of temperature (and the concentrations of various species) become small, and our model reduces to the lumped-parameter model presented earlier[6]. *Figure 17* clearly shows that neglecting the radial variations leads to very different results. *Figures 18–21* show how the results for $\bar{x}$, $\overline{\mu_n}$, $\bar{Q}$ and $\overline{[C_2]}$ are also quite different for the $k \to \infty$ case (lumped model results) when compared to the results from the present model, where the radial gradients are correctly accounted for. The importance of accounting for these effects is clearly seen. The use of the lumping approximation in such reactors could lead to errors in design, particularly if one were interested in using the model for control-system design, or for optimization.

CONCLUSIONS

An energy-efficient autothermal industrial nylon-6 reactor is simulated under steady-state conditions, using a model that accounts for radial variations of temperature and concentrations of molecular species. The results show that accounting for these radial variations is extremely important, and a lumped model could lead to faulty designs. It is found that the hot-spot temperature in this reactor is parametrically sensitive to the feed-water concentration, and to the presence of monofunctional acids in the feed stream. The effects of varying the

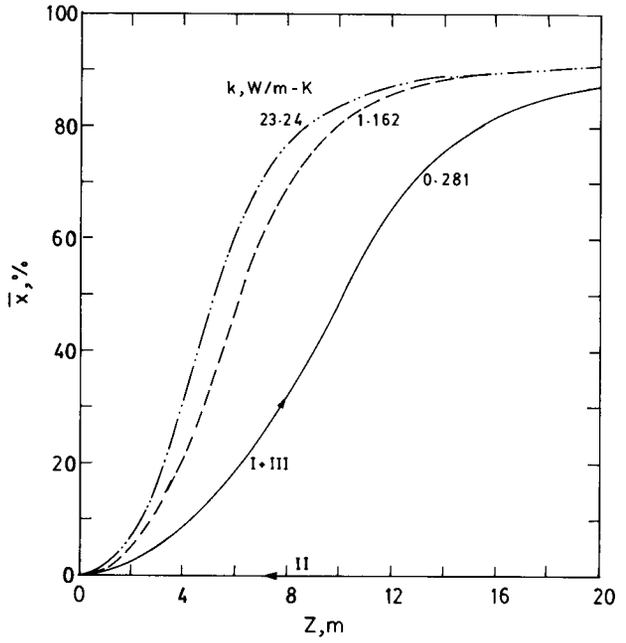

Figure 18 Effect of increasing k on $\bar{x}$

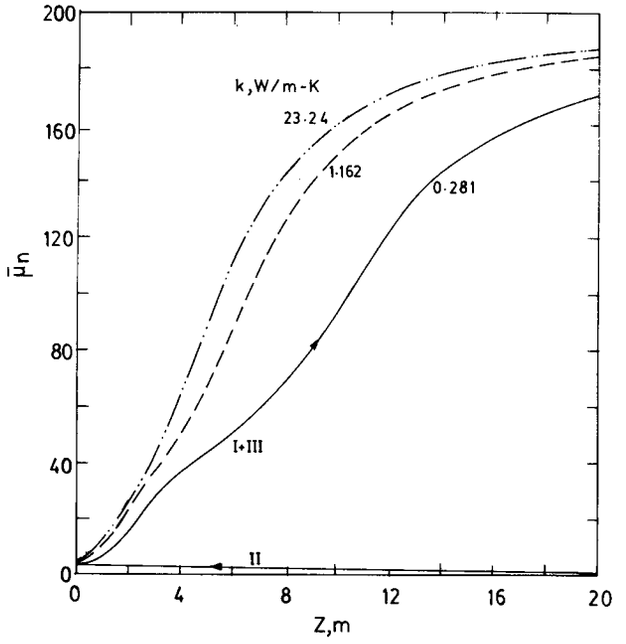

Figure 19 Effect of increasing k on $\bar{\mu}_n$

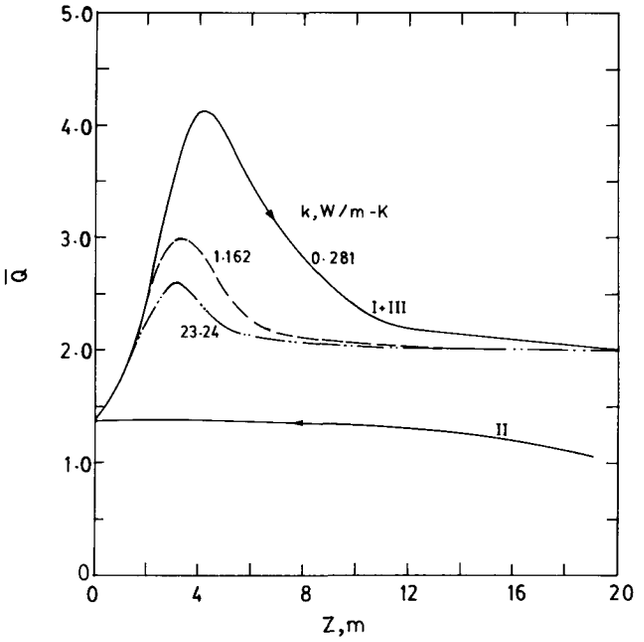

Figure 20 Effect of increasing k on $\bar{Q}$

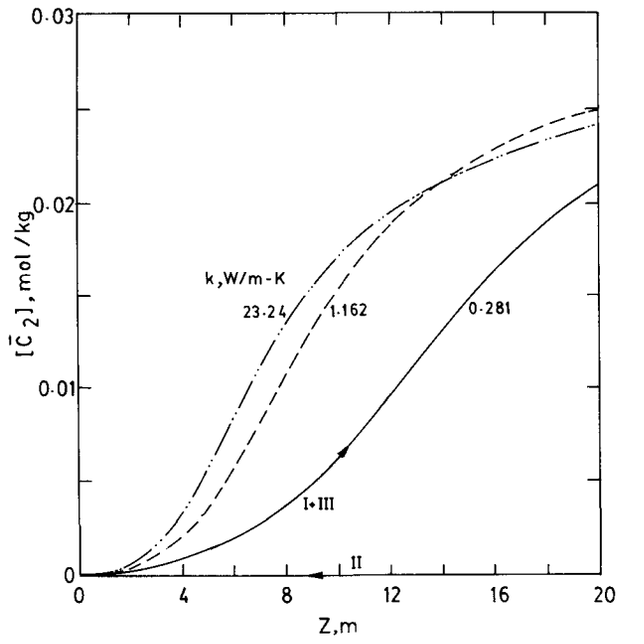

Figure 21 Effect of increasing k on $\overline{[C_2]}$

important operating conditions are also studied. From this reactor, one can obtain a product having the same number-average molecular weight using two different feed-water concentrations. In addition, our study emphasizes the need for having good estimates of the inside heat transfer coefficients, U_1 and U_2.

REFERENCES

1 Reimschuessel, H. K. *J. Polym. Sci., Macromol. Rev.* 1977, **12**, 65
2 Tai, K. and Tagawa, T. *Ind. Eng. Chem., Prod. Res. Dev.* 1983, **22**, 192
3 Gupta, S. K. and Kumar, A. 'Reaction Engineering of Step Growth Polymerization', Plenum, New York, 1987
4 Gupta, S. K. 'Handbook of Polymer Science and Technology', Vol. 1 (Ed. N. P. Cheremisinoff), Dekker, New York, 1989, p. 211
5 Sittig, M. 'Polyamide Fiber Manufacture', Noyes Data Corp., Park Ridge, NJ, 1972
6 Gupta, S. K. and Tjahjadi, M. *J. Appl. Polym. Sci.* 1987, **33**, 933
7 Gupta, A., Gupta, S. K., Gandhi, K. S., Ankleswaria, B. V., Mehta, M. H., Padh, M. R. and Soni, A. 'Recent Trends in Chemical Reaction Engineering' (Eds. B. D. Kulkarni, R. A. Mashelkar and M. M. Sharma), Wiley, New Delhi, 1987, p. 281
8 Gupta, A., Gandhi, K. S., Gupta, S. K., Mehta, M. H., Padh, M. R., Soni, A. V. and Ankleswaria, B. V. *Chem. Eng. Commun.* 1992, **113**, 63
9 Ramgopal, A., Kumar, A. and Gupta, S. K. *Polym. Eng. Sci.* 1982, **22**, 849
10 Pal, D. and Gupta, S. K. *Polymer* 1989, **30**, 1918
11 Jacobs, H. and Schweigman, C. Proc. 5th Eur./2nd Int. Symp. Chemical Reaction Engineering, Amsterdam, 2–4 May 1972
12 Bird, R. B., Stewart, W. E. and Lightfoot, E. N. 'Transport Phenomena', Wiley, New York, 1960
13 Gupta, V. and Gupta, S. K. 'Fluid Mechanics and its Applications', Wiley, New Delhi, 1984
14 Hamer, J. W. and Ray, W. H. *Chem. Eng. Sci.* 1986, **41**, 3083
15 Finlayson, B. A. 'Nonlinear Analysis in Chemical Engineering', McGraw-Hill, New York, 1980
16 Ray, A. K. and Gupta, S. K. *J. Appl. Polym. Sci.* 1985, **30**, 4529

NOMENCLATURE

A_i	Frequency factor of uncatalysed ith reaction ($kg\ mol^{-1}\ h^{-1}$); also, area of cross-section of reactor i (m^2)
A_i^c	Frequency factor of ith catalysed reaction ($kg^2\ mol^{-2}\ h^{-1}$)
A_n	Monofunctional polymer
C_1	Caprolactam
C_2	Cyclic dimer
C_p	Specific heat of reaction mass ($J\ kg^{-1}\ K^{-1}$)
E_i	Activation energy of ith uncatalysed reaction ($J\ mol^{-1}$)
E_i^c	Activation energy of ith catalysed reaction ($J\ mol^{-1}$)
ΔH_i	Heat of reaction ($J\ mol^{-1}$)
k	Thermal conductivity of reaction mass ($W\ m^{-1}\ K^{-1}$)
k_i	Rate constant for forward reaction ($kg\ mol^{-1}\ h^{-1}$)
k_i'	Rate constant for backward reaction ($kg\ mol^{-1}\ h^{-1}$)
K_i	Equilibrium constant of ith reaction
L	Length of reactor (m)
Q	Polydispersity index $\equiv (\mu_2 + \mu_2')(\mu_0 + \mu_0')/(\mu_1 + \mu_1')^2$
r	Radial position (m)
R	Universal gas constant ($J\ mol^{-1}\ K^{-1}$)
R_i	Radius of reactor i (m)
$R_{r,i}$	Net forward rate of ith reaction ($mol\ kg^{-1}\ h^{-1}$)
S_n	Bifunctional polymer molecule having n repeat units
ΔS_i	Entropy of ith reaction ($J\ mol^{-1}\ K^{-1}$)
T	Temperature (K)
U_i	Overall heat transfer coefficient ($W\ m^{-2}\ K^{-1}$)
V_i	Velocity at any r and Z in reactor i ($m\ h^{-1}$)
$\bar{V}_i$	Average velocity in reactor i ($m\ h^{-1}$)
W	Water
x	Monomer conversion
Z	Axial location (m)

Greek letters

μ_k kth moment of bifunctional species (mol kg^{-1}) $\equiv \sum_{n=1}^{\infty} n^k[S_n]$, $k = 0, 1, 2, \ldots$

μ'_k kth moment of monofunctional species (mol kg^{-1})

μ_n Number-average chain length $= (\mu_1 + \mu'_1)/(\mu_0 + \mu'_0)$

ρ Density of reaction mass (kg m^{-3})

$\xi_{i,j}$ Concentration of ith species (or moment) in reactor j (mol kg^{-1}) (defined in *Table 3*)

$\dot{\xi}_i$ Rate of production of ξ_i (mol kg^{-1} h^{-1})

Subscripts

f Feed condition

j Jacket

end Outlet of the autothermal reactor

Symbols

[ ] Molar concentrations (mol kg^{-1})

$\overline{\ }$ Spatially (radially) averaged value